



HAL
open science

Cavitation simulation using a new simple homogeneous cavitation model

Satoshi Watanabe, Wakana Tsuru, Yuya Yamamoto, Shin-Ichi Tsuda

► **To cite this version:**

Satoshi Watanabe, Wakana Tsuru, Yuya Yamamoto, Shin-Ichi Tsuda. Cavitation simulation using a new simple homogeneous cavitation model. 16th International Symposium on Transport Phenomena and Dynamics of Rotating Machinery, Apr 2016, Honolulu, United States. hal-01890084

HAL Id: hal-01890084

<https://hal.science/hal-01890084>

Submitted on 8 Oct 2018

HAL is a multi-disciplinary open access archive for the deposit and dissemination of scientific research documents, whether they are published or not. The documents may come from teaching and research institutions in France or abroad, or from public or private research centers.

L'archive ouverte pluridisciplinaire **HAL**, est destinée au dépôt et à la diffusion de documents scientifiques de niveau recherche, publiés ou non, émanant des établissements d'enseignement et de recherche français ou étrangers, des laboratoires publics ou privés.

Cavitation simulation using a new simple homogeneous cavitation model

Satoshi Watanabe^{1*}, Wakana Tsuru², Yuya Yamamoto², Shin-ichi Tsuda²



Abstract

In this paper, preliminary simulations of cavitating flows in two cases, for a two-dimensional convergent-divergent nozzle and a two-dimensional Clark Y-11.7% hydrofoil, are carried out based on our new simple homogeneous cavitation model. The model treats liquid-vapor two-phase flows as usual homogeneous cavitation model but it considers two extreme conditions; the bubbly flow with dispersed bubbles in continuous liquid phase and mist flow with dispersed liquid droplets in continuous vapor phase, which are switched depending upon the local volumetric fraction of two phases, i.e. the void fraction. To enhance the unsteadiness due to the instability at the cavity interface, the turbulent shear stress is modified based on the fluid properties of continuum phase. The results are compared to the previous experimental measurements and the results simulated with Schnerr-Sauer cavitation model. It is found that turbulent shear stress has important effects on cavitation unsteadiness. However, time-averaged lift and drag characteristics of hydrofoil against cavitation are not well reproduced regardless of cavitation model and turbulence modification.

Keywords

Homogeneous cavitation model - Turbulent viscosity - Convergent-divergent nozzle - Clark Y hydrofoil

¹Department of Mechanical Engineering, Kyushu University, Fukuoka, Japan

²Graduate School of Engineering, Kyushu University, Fukuoka, Japan

*Corresponding author: fmnabe@mech.kyushu-u.ac.jp

INTRODUCTION

Cavitation phenomena and its unsteadiness have been widely studied to further improve the performance of fluid machinery. Numerical simulation considering cavitation is becoming popular in the design stage of fluid machinery. Many cavitation models have been developed [1]-[3], and have contributed to qualitative, and in some extent, quantitative predictions of cavitating flow. However, even in simple cases of cavitating single hydrofoil, they often fail to predict the cavitation performance (Kato [4]). Moreover, although RANS (Reynolds-Averaged Navier-Stokes) model for turbulent flow simulation is often used to simulate unsteady cavitating flow, a re-entrant jet can never be reproduced with RANS. It is difficult without any special treatments to reproduce the unsteadiness of cavitation.

Reboud et al. [5] has proposed the well-known Reboud's correction which cuts the turbulent viscosity in the two phase flow region to avoid an overestimation of the eddy viscosity in this region. By using this correction method, the cavitation unsteadiness in cases of a two-dimensional convergent-divergent nozzle [5], a two-dimensional hydrofoil [6] and a three-dimensional twisted hydrofoil [7] have been successfully reproduced. This correction method is very effective but still more or less empirical, therefore, the development of cavitation model with the robust prediction accuracy is still an important issue.

In the above background, a new simple homogeneous cavitation model has been proposed in our previous study [8]. Unlike usual homogeneous cavitation model where the dilute vapor bubbly flow is assumed in all two-phase flow region even with high void fraction (vapor volumetric fraction), the model considers two extreme conditions of two-phase

mixture, dispersed vapor bubbles in continuous liquid phase and dispersed liquid droplets in continuous vapor phase and switches these two two-phase configuration depending on the local void fraction. With this proposed model, it can be easier to recognize the cavity interface and the cavitating flow region, therefore new modeling of turbulence is also expected to be easily in-cooperated. In this study, the modification of the turbulent viscosity in two-phase flow regions similar to Reboud's correction but in a different way is implemented, to enhance the unsteadiness of cavitation.

In the present study, cavitation simulations with the proposed homogeneous cavitation model is preliminarily carried out for two two-dimensional geometries, a convergent-divergent nozzle and around a single Clark Y-11.7% hydrofoil, to validate the model as well as to figure out the remaining problems.

1. METHODS

1.1 Solver and models

In the present study, an open source C++ library, OpenFOAM-2.2.1, is used, and interPhaseChangeFoam (IPCF) in which several cavitation models are implemented is employed as a base solver. IPCF is a homogeneous cavitating flow solver based on an incompressible Navier-Stokes (NS) equation with considering the mass transfer between liquid and vapor phases. In addition to the usual sets of NS equations for the two-phase mixture and the transport equations of turbulence properties, the IPCF solves the following mass conservations of mixture and liquid phase,

$$\frac{\partial u_j}{\partial x_j} = \left(\frac{1}{\rho_l} - \frac{1}{\rho_v} \right) (\dot{m}^+ + \dot{m}^-) \quad (1)$$

$$\frac{\partial \alpha_l}{\partial t} + \frac{\partial \alpha_l u_j}{\partial x_j} = \frac{1}{\rho_l} (\dot{m}^+ + \dot{m}^-) \quad (2)$$

where x_j is a Cartesian coordinate, u_j a velocity component in x_j direction, ρ_l and ρ_v the liquid and vapor densities, and α_l the liquid volume fraction. The vapor volume fraction, that is a void fraction, can be calculated by $\alpha_v = 1 - \alpha_l$. The mass transfer rates between two phases, \dot{m}^+ and \dot{m}^- , due to condensation and evaporation should be modelled to close the problem. In this study, the following two models are used.

1.1.1 Schnerr-Sauer (SS) model [9]

Schnerr-Sauer (SS) model implemented in OpenFOAM-2.2.1 has been used in many studies [10, 11]. In this study, SS model is also employed for the base of the proposed model. The SS model considers vapor bubbles as dispersed phase in continuum liquid phase in all two-phase flow regions regardless of the local void fraction. The SS model is derived from Rayleigh-Plesset equation, which describe growth/shrink of a single spherical bubble;

$$R \frac{d^2 R}{dt^2} + \frac{3}{2} \left(\frac{dR}{dt} \right)^2 = \frac{p - p_v}{\rho_l} \quad (3)$$

where R is a bubble radius, p and p_v local and vapor pressures. When the first term on the left side of Eq. (3) is assumed to be negligible, the bubble radius growth can be represented by the following equation.

$$\frac{dR}{dt} = \text{sign}(p_v - p) \sqrt{\frac{2 |p - p_v|}{3 \rho_l}} \quad (4)$$

Assuming that the number density of bubble nuclei, n_{nuc} , that is the number of nuclei in a unit liquid volume, is constant, i.e. no generation, destruction, coalescence nor break up occur, we can relate the local bubble radius with the local void fraction as follows.

$$\alpha_v = \frac{n_{nuc} \frac{4\pi}{3} R^3}{1 + n_{nuc} \frac{4\pi}{3} R^3} \quad (5)$$

$$R = \sqrt[3]{\frac{\alpha_v}{\frac{4}{3} \pi n_{nuc} (1 - \alpha_v)}} \quad (6)$$

From those equations, the mass source terms of SS model is obtained as follows.

$$\dot{m}^+ = C_c \frac{\rho_v \rho_l}{\rho} \alpha_v (1 - \alpha_v) \frac{3}{R} \sqrt{\frac{2(p - p_v)}{3 \rho_l}} \quad (p > p_v) \quad (7)$$

$$\dot{m}^- = -C_e \frac{\rho_v \rho_l}{\rho} \alpha_v (1 - \alpha_v) \frac{3}{R} \sqrt{\frac{2(p_v - p)}{3 \rho_l}} \quad (p < p_v) \quad (8)$$

where C_c and C_e are condensation and evaporation coefficients respectively, and $\rho = \rho_l \alpha_l + \rho_v \alpha_v$ the mixture density. In the present study, the basic parameters in this

model are set as $n_{nuc} = 1.6 \times 10^{13} \text{ m}^{-3}$, and $C_c = C_e = 1.0$.

1.1.2 Bubble-Droplet 1 model [8]

Most of homogeneous cavitation models already proposed considers mass transfer through surfaces of dilute tiny bubbles, although the application of such dispersed bubble model for large void fraction regions seems to be inappropriate. In this model, another extreme case in which vapor phase contains more or less liquid droplets is considered. When the local void fraction is close to unity, vapor phase is treated as a continuum media, and mass transfer through surfaces of dilute tiny droplets is considered, as shown in Fig. 1. This model virtually considers the interface between liquid and vapor phases as the iso-surface of void fraction $\alpha_{v,int}$, and in this study $\alpha_{v,int}$ is set to be 0.5 for simplicity.

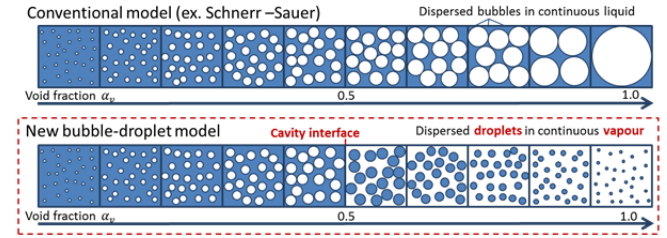


Fig.1 Conceptual drawing of bubble droplet model [8]

The mass transfer between vapor and liquid are dominated by that occurs at the surfaces of the bubbles/droplets, then the mass transfer rates $\dot{m}^+ + \dot{m}^-$ are switched depending upon the local void fraction α_v . In the proposed model "Bubble-Droplet 1", bubbly flow model similar to SS model, i.e. Eqs. (7) and (8), is adopted for the local region with $\alpha_v < \alpha_{v,int}$, while for $\alpha_v > \alpha_{v,int}$, the phase change at the surface of droplet is considered, simply using Schrage's mass flux \dot{M} [12], expressed as follows

$$\dot{M} = \frac{k}{\sqrt{2\pi R_g T}} (p_v - p) \quad (9)$$

where k is a evaporation/condensation coefficient, R_g a gas constant, and T temperature. The value of k is set to 0.4 throughout the present computations. By considering the phase change through the total surface area of droplets, the mass transfer rate can be obtained as

$$\dot{m} = \dot{m}^+ + \dot{m}^- = -\frac{k}{\sqrt{2\pi R_g T}} \frac{3(1 - \alpha_v)}{R_d} (p_v - p) \quad (10)$$

where R_d is a radius of droplet, which can be calculated with the assumption of the constant number density of droplet per unit volume of vapor by

$$R_d = \sqrt[3]{\frac{\alpha_l}{\frac{4}{3} \pi n_{nuc} (1 - \alpha_l)}} = \sqrt[3]{\frac{1 - \alpha_v}{\frac{4}{3} \pi n_{nuc} \alpha_v}} \quad (11)$$

Since the cavity interface can be virtually treated, the mass transfer at the cavity interface is supposed to be possibly treated, which remains for our future study.

1.1.3 Turbulence modification

Key unsteady cavitation phenomena such as a re-entrant jet which develops beneath the sheet cavity and a resultant formation of cloud cavity can never be simulated with incompressible RANS turbulence model. However, it is still used for simplicity, and to enhance the unsteadiness due to the instability on the sheet cavity interface, we switch the eddy viscosity as well as the molecular viscosity by referring only the continuum phase. The eddy viscosity, μ_t , and the molecular viscosity, μ , of two-phase mixture are respectively calculated by following Eqs. (12) and (13).

$$f(\alpha_v) = \frac{\rho_l + \rho_v}{2} - \frac{\rho_l - \rho_v}{2} \tanh\left(\frac{\alpha_v - \alpha_{v,int}}{\Delta\alpha}\right) \quad (12)$$

$$\mu = \frac{\mu_l + \mu_v}{2} - \frac{\mu_l - \mu_v}{2} \tanh\left(\frac{\alpha_v - \alpha_{v,int}}{\Delta\alpha}\right) \quad (13)$$

where μ_l and μ_v are the molecular viscosities of liquid and vapor phases, $\mu_{t,org}$ is the turbulent viscosity originally calculated by RANS turbulence model, for which standard $k - \varepsilon$ model or Shear Stress Transport (SST) model is employed in the present study. By employing another parameter $\Delta\alpha$, we can define the thickness of the interface of cavity, the value of which is fixed to 0.1 throughout this study.

This treatment may look similar to well-known Rebound correction [5], while in this study the turbulent and molecular viscosities are modified based on the fluid properties of continuum phase only as shown in Fig. 2, which is suitably applied in combination with our proposed cavitation model.

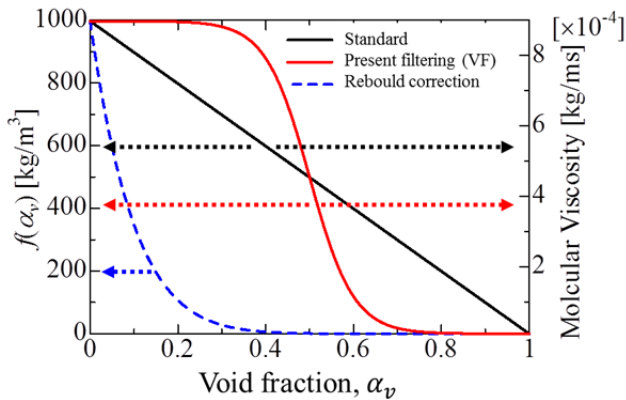


Fig.2 Comparison of viscosity

2. Simulation of 2-D convergent-divergent flow

2.1 Model description

Two-dimensional numerical simulation has been carried out for unsteady cavitating flow in the two-dimensional convergent-divergent nozzle as shown in Fig. 3 [8]. The results of numerical simulation will be briefly introduced in the following sub-section.

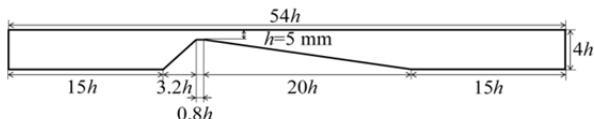


Fig.3 Computational domain of nozzle

The height of the nozzle throat, h , is 5mm. The angles of the convergent and divergent parts are 43 and 8.4 degrees, respectively. The velocity is fixed at the inlet ($U_{inlet} = 1.5\text{m/s}$), and the static pressure is fixed at the outlet. The non-slip condition is applied on the upper and lower walls of the nozzle. The number of cells is 72,000. The second order upwind scheme is used for the convection scheme except for that for the liquid volume fraction, for which Van Leer TVD scheme is employed. Implicit Euler scheme is applied for the time integration, and the maximum CFL (Courant) number is set to be 0.8. Standard $k - \varepsilon$ turbulence model is employed for the base turbulence model. The viscosity modification by Eqs. (12) and (13) are applied only for BD1 model (here we call BD1VF model).

2.2 Results

Figure 4 (a) shows the cavity shapes observed by the previous experiment [13]. The computational results with similar cavity length for SS and BD1VF models are shown in Figs. 4 (b) and 4 (c), respectively. The time interval in these figures is 4ms. The cavitation number is defined as

$$\sigma = \frac{p_{in} - p_v}{\rho_l U_{inlet}^2 / 2} \quad (11)$$

where p_{in} is the time-averaged inlet static pressure.

It should be noted that the cavitation numbers giving the similar cavity lengths are very different between the experiment (1.14) and the simulations (0.49 for SS model and 1.63 for BD1VF model). One of the reasons for this may be due to the 2-D flow simulation with low Reynolds number flow. The Reynolds number based on the nozzle throat height and the area averaged velocity there is $Re = U_{nozzle} h / \nu \cong 3 \times 10^4$. The blockages due to the wall boundary layers are to be very sensitive to the Reynolds number itself as well as the domain size, and the pressure difference between upstream and at the nozzle throat is hard to be accurately predicted with the small throat height of h .

Focusing on the unsteadiness of cavitation, the fluctuations of cavity shape can be seen at the tail part of cavity in SS model (Fig. 4(b)), whereas no cloud cavities are found. On the other hand, the cloud cavitation can be seen in BD1VF model (Fig. 4(c)), and the behavior is similar to the experiment (Fig.4(a)). It can be said that the turbulent shear stress has very important effects on the unsteadiness of cavitation.

Figure 5 shows the results of the FFT analysis of pressure fluctuation at 23h downstream from the throat on the upper wall. In this figure, it can be seen that the strong peak is found at 60Hz in the case of SS and at 45Hz in the case of BD1VF, and the amplitude of other components is larger in BD1VF model than is SS model in the all frequency range. It is inferred from the observation that the continuous cloud cavity shedding from the tail part of sheet cavity causes the pressure fluctuations at wide range of the frequency. These trends are found in other cavitation number conditions.

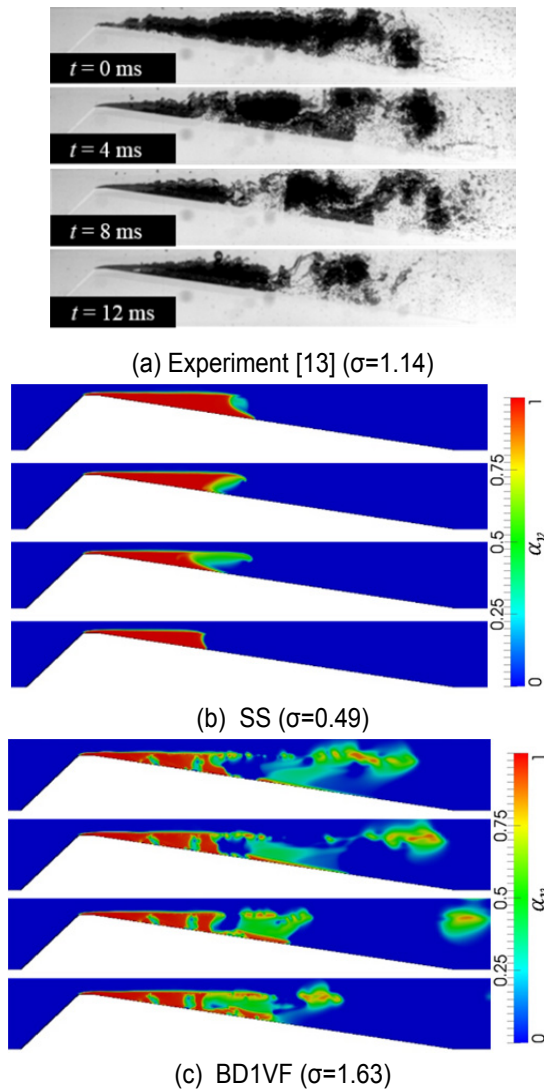


Fig. 4 Instantaneous cavity shapes in the experiment [13] and present simulations (time interval :4ms)

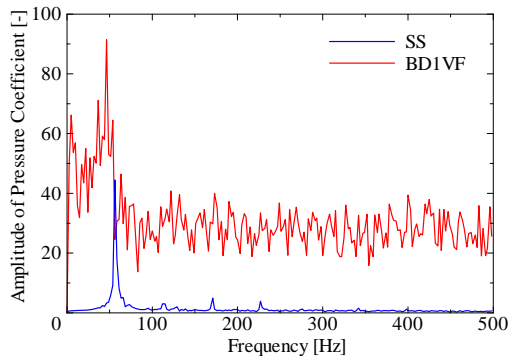


Fig. 5 Comparison of frequency spectra of pressure fluctuation between two cavitation models

3. Simulation of flow around 2-D Clark Y hydrofoil

3.1 Model description

In this section, two-dimensional numerical simulation is carried out for unsteady cavitating flow around two-dimensional Clark Y-11.7% hydrofoil shown in Fig. 6.

The examined hydrofoil has the chord length of $C = 100$ mm and is located at the center of the domain. The height of computational domain is $2C$, which is identical to the tunnel

height of our previous experiment [14]. The inlet and outlet boundaries locate at $5C$ upstream and downstream from the mid chord location of the hydrofoil, as shown in Fig. 7. The total number of cells is 232,818. The angle of attack is set to be 8 degrees, at which it is known that the laminar separation bubble is formed near the leading edge of the hydrofoil in non-cavitating condition.

As the boundary conditions, the velocity is fixed at the inlet as $U_{in} = 8.1\text{m/s}$, and the static pressure is specified at the outlet to set the cavitation number. The non-slip condition is applied on the hydrofoil surface, but to reduce the number of grid cells far from the hydrofoil, the slip condition is applied on the upper and lower walls. The second order upwind scheme is used for the convection scheme except for that for the liquid volume fraction, for which Van Leer TVD scheme is employed. Implicit Euler scheme is applied for the time integration, and the time step is set to $0.5 \times 10^{-6}\text{s}$. This time, $k - \omega$ based SST turbulence model is employed, and the viscosity modification by Eqs. (12) and (13) are applied for both SS and BD1 models since it has been found to be effective for the reproduction of unsteadiness of cavitation.

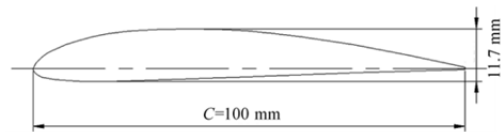


Fig.6 Clark Y-11.7% hydrofoil

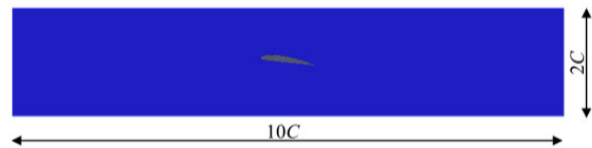


Fig.7 Computational domain

3.2 Results

Figure 8 shows (a) the time-averaged lift coefficient, $C_L = L/(\rho U^2 BC/2)$, and (b) the drag coefficient, $C_D = D/(\rho U^2 BC/2)$ against the cavitation number σ , obtained by the previous experiment [14] and the present simulations with SS and BD1VF models. B is the span of the hydrofoil and $B = 81.0\text{mm}$ in the referred experiment. In the experiment, the sufficient time duration is taken to obtain the time averaged data, whereas only about 0.5s is used for the simulations to present the preliminary results. The cavitation number for this simulation is defined as

$$\sigma = \frac{p_{ref} - p_v}{\rho_l U_{in}^2 / 2} \quad (15)$$

where p_{ref} is the reference pressure and upstream pressure is used for the experiment but the pressure at the outlet boundary is used for the present simulations. It should be noted that the pressure difference between upstream and downstream is small because of the small drag force of the hydrofoil.

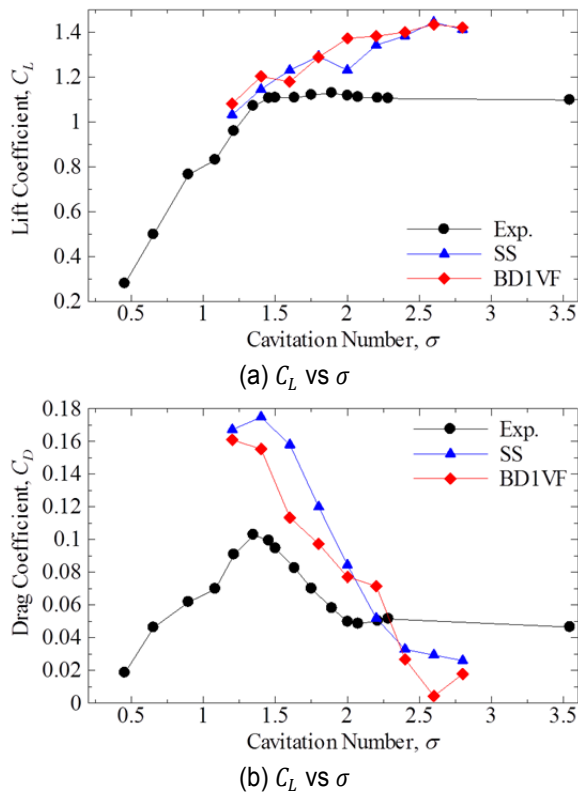


Fig. 8 Lift and drag coefficients of Clark Y hydrofoil against cavitation number

From Fig 8, it can be seen that the both lift and drag coefficients C_L and C_D are different between the experiment and the numerical simulations even at large cavitation number case ($\sigma = 2.8$) with small amount of cavitation. This is believed to be due to 2-D model in the present simulations. The blockage effect of upper and lower walls as well as the end wall (blade roots) effect in the experiment is the reason for it. The tendency of C_L and C_D against the development of cavitation, i.e. the decrease of σ , are similar between two models SS and BD1 models, but both of them are different from the experimental result. Especially in the experiment, C_L slightly increases in $\sigma = 1.5 - 2.0$ with the development of cavitation but in the both two cavitation models, it starts to decrease around $\sigma = 2.5$, which is much faster than the experiment. And also the drag coefficient C_D starts to increase at larger cavitation number in the numerical simulations than that in the experiment and the maximum value is larger for the numerical simulations, although the numerical results are a little scattered due to insufficient time duration to obtain the time averaged value. Therefore, although it is difficult to justify the present models from the presented data, there should apparently be something to be made for the accurate prediction of lift and drag forces in cavitating conditions.

Figure 9 shows the lift coefficient fluctuations obtained by the experiment ($\sigma = 1.45$) and by the present simulations with (b) SS model ($\sigma = 1.40$) and (c) BD model ($\sigma = 1.40$). In all results, the periodic fluctuation of lift coefficient can be seen, but the clearer periodicity can be found for the experiment. However, the amplitude of the fluctuation is much larger in the numerical simulations than in the experiment. Fig. 10 shows the instantaneous cavity shapes

during one cycle of fluctuation. The static pressure distributions are also shown for the numerical simulations. The times of A to H in Fig. 10 correspond to those marked in Fig. 9. In the experiment, it can be seen that the large two-dimensional sheet cavity is formed and at the instant C the large cloud cavity is detached from the sheet cavity, and is convected along the suction surface. At G-H, the cloud cavity reaches the trailing edge of the hydrofoil, and the lift coefficient drops simultaneously. In the numerical simulations with the both two models, the development of sheet cavity at A-E, the formation and the convection of the cloud cavity at B to H, and the lift drop at G-H are well reproduced. The lift drop is caused by the cloud cavity passing near the trailing edge of the hydrofoil. Then, it might be said that the unsteadiness of cavitation is qualitatively reproduced by the present cavitation model with the modification of the turbulence model.

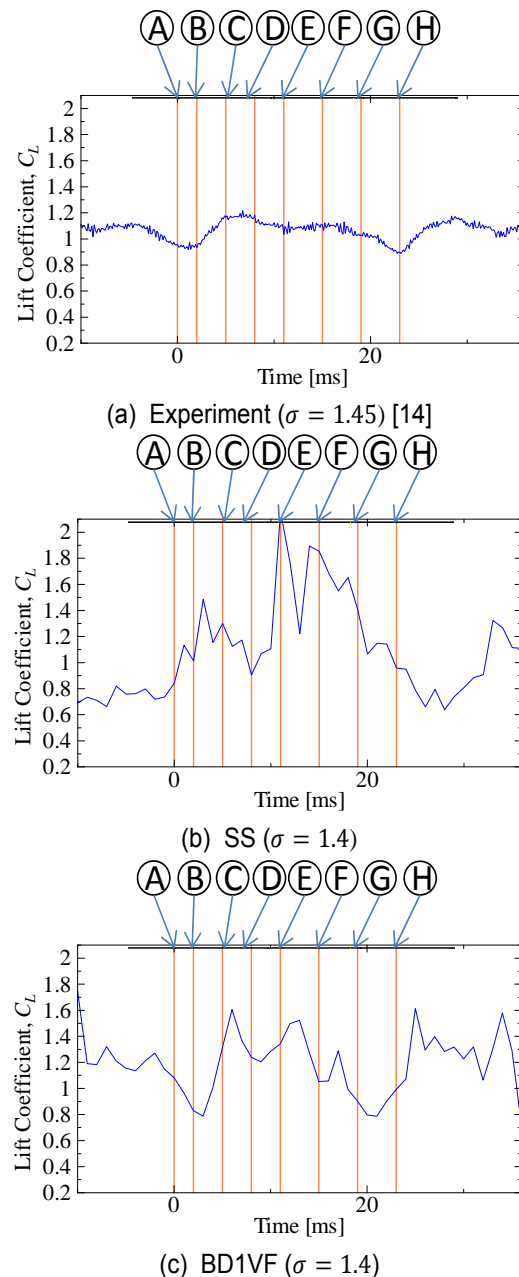


Fig. 9 Instantaneous lift coefficient in cavitation conditions with $\sigma = 1.4 - 1.45$

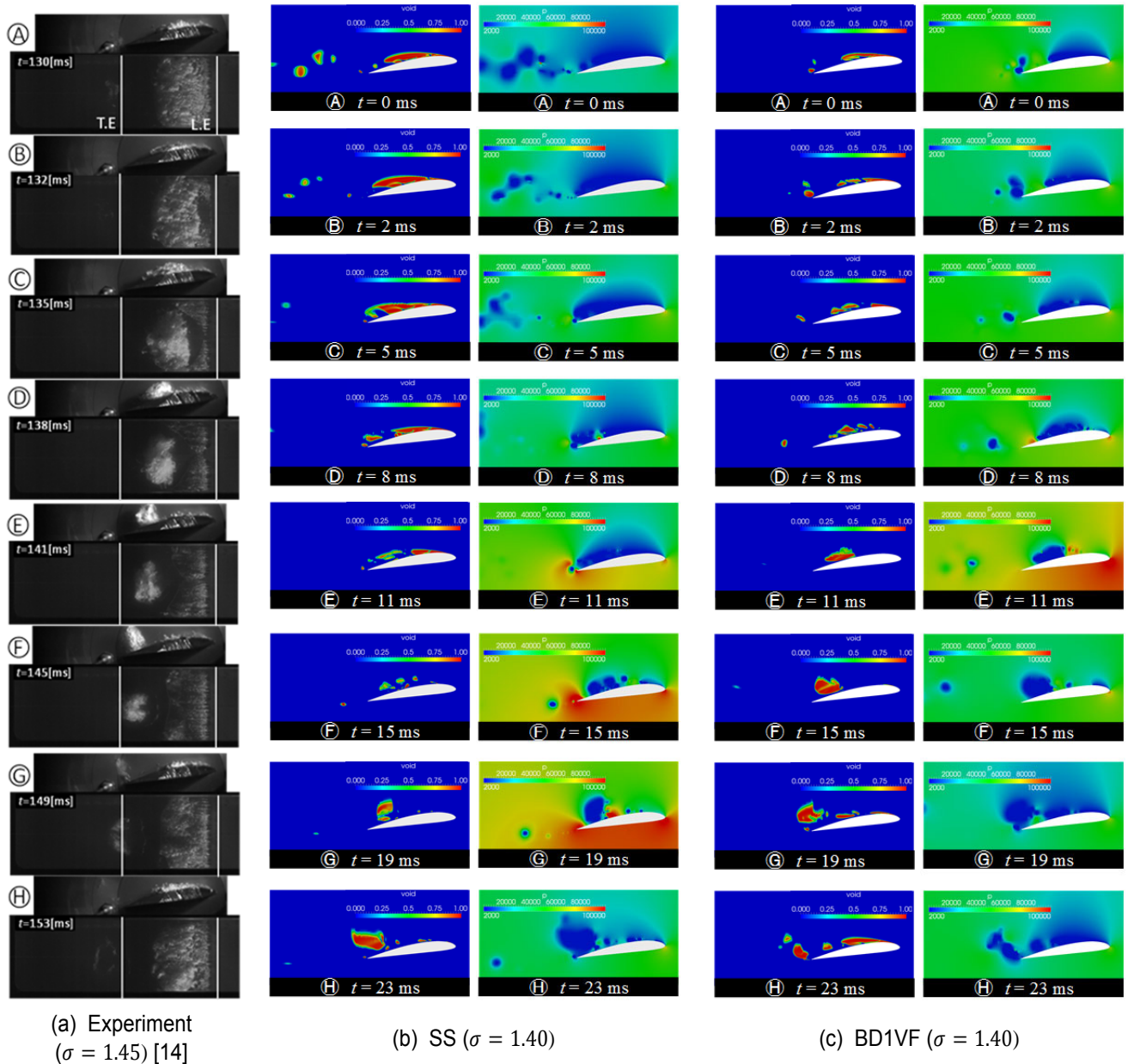


Fig.10 Comparisons of instantaneous cavity shapes around hydrofoil among numerical models and experiment. Corresponding pressure distributions are also shown for numerical simulations

However, the detailed flow structure is still quantitatively different from that observed in the experiment; for example, the sheet cavity diminishes just after the complete release of the cloud cavity (G for SS and E for BD1VF) only in the results of numerical simulations, which may result in the larger lift/drag force fluctuations. This may be caused by the same defect of the present cavitation model in-cooperated with RANS turbulence model.

Figure 11 shows the time averaged pressure distributions around the hydrofoil for (a) SS model and (b) BD1VF model. The experimental data [15] are also plotted with symbols in the both figures for comparisons. Pressure coefficient C_p is defined as $C_p = 2(p - p_{ref})/(\rho_l U_{in}^2/2)$. The negative suction peak appears with its larger value in numerical simulations, which results in the early cavitation inception; even at $\sigma=2.8$, stable leading edge cavitation forms in the numerical simulations. If we compare the pressure distributions between CFD and the experiments, it can be

seen that the numerical results at $\sigma=2.0$ for the both models are similar to the experimental one at $\sigma=1.64$, which indicates that the time averaged cavity length is longer for numerical simulation, probably due to the difference of the suction peak between the numerical simulations and the experiment. It is also interesting to see that the time averaged pressure on the suction side C_p takes larger than $-\sigma$ at $\sigma=1.6$ in the numerical simulations. This means that the time-averaged pressure in the cavitating zone is larger than vapour pressure. This is probably due to the strong large-scale unsteadiness of cavitation. As has been seen in Fig.10, just after the complete formation of cloud cavity (G for SS model and E for BD1VF model), the pressure on the suction side is very large compared with vapor pressure except for the cloud cavity region. Although the examined cavitation number between Figs.10 and 11 is different, this instantaneous pressure rise seems to be responsible for the large C_p values than $-\sigma$ in the numerical simulations.

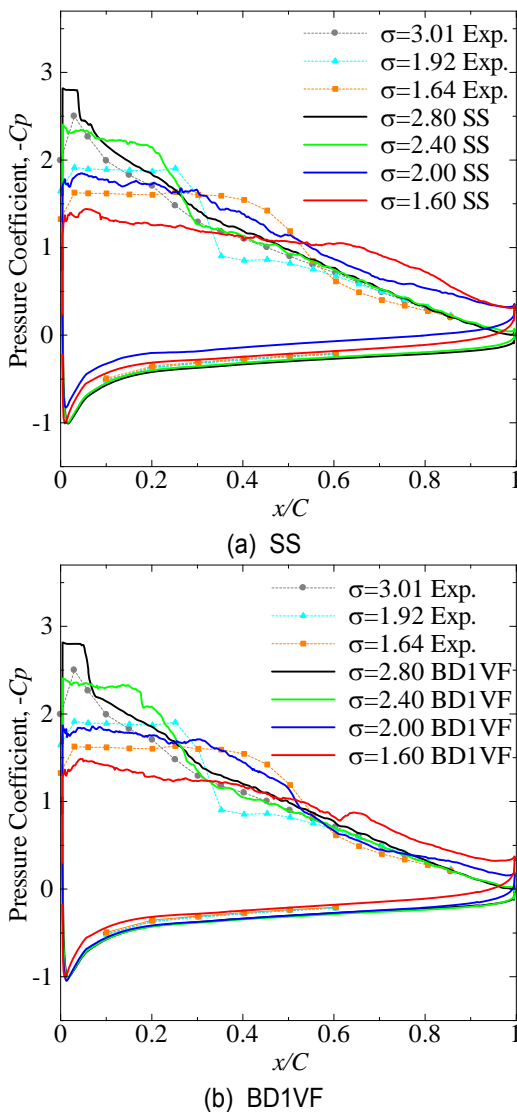


Fig. 11 Time-averaged pressure distributions around hydrofoil for various cavitation numbers

4. Conclusion

In this paper, preliminary simulations of cavitating flows in two cases, for a two-dimensional convergent-divergent nozzle and a two-dimensional Clark Y-11.7% hydrofoil, are carried out based on our new simple homogeneous cavitation model. The model treats liquid-vapor two-phase flows as usual homogeneous model but it considers two extreme conditions; the bubbly flow with dispersed bubbles in continuous liquid phase and mist flow with dispersed liquid droplets in continuous vapor phase, which are switched depending upon the local void fraction. To enhance the unsteadiness due to the instability at the cavity interface, the turbulent shear stress is modified based on the fluid properties of continuum phase. The results are compared to the previous experimental measurements and the results simulated with Schnerr-Sauer cavitation model.

In the simulation of the nozzle flow, the cloud cavity can be seen in results of the new cavitation model in-cooperated with the turbulence modification, and the behavior is similar to the experiment. It can be said that the turbulent shear stress has important effects on unsteadiness of cavitating flow.

In the simulation of cavitating flow around Clark Y-11.7% hydrofoil, it is found that the time-averaged lift and drag coefficients and the cavity length are not very affected by the cavitation model. The unsteady nature of cavitating flow such as the cloud cavity formation seems to be qualitatively reproduced by the present 2-D simulation, but the quantitatively different. Those may be caused by the same defect of the present cavitation model in-cooperated with RANS turbulence model.

The present computations have been mainly carried out using the computer facilities at Research Institute for Information Technology, Kyushu University, Japan.

References

- [1] R. F. Kunz, D. A. Boger, D. R. Stinebring, T. S. Chyczewski, J. W. Lindau, H. J. Gibeling, S. Venkateswaran, T. R. Govindan. A Preconditioned Navier-Stokes Method for Two-Phase Flows with Application to Cavitation Prediction. *Computers & Fluids*, Vol. 29, 849-875, 2000.
- [2] C. L. Merkle, K. Feng, and P. E. Below. Computational Modeling of the Dynamics of Sheet cavitation. *Proc. the 3rd International Symp. on Cavitation*, Grenoble, France, Vol. 2, 47-54, 1998.
- [3] P. K. Zwart, A. G. Gerber and T. Belamri. A Two-Phase Flow Model for Predicting Cavitation Dynamics, *Proc. the Fifth Int. Conf. on Multiphase Flow*, Yokohama, Japan, 2004.
- [4] C. Kato. Industry-University Collaborative Project on Numerical Predictions of Cavitating Flows in Hydraulic Machinery - part I: Benchmark test on cavitating hydrofoils-. *Proc. ASME-JSME-KSME Joint Fluids Engineering Conf.* 2011, AJK2011-06084
- [5] J. L. Reboud, B. Stutz, and O. Goutier. Two-Phase Flow Structure of Cavitation: Experiment and Modeling of Unsteady Effects. *Proc. Third International Symp. on Cavitation*, 203-208, 1998
- [6] O. Coutier-Delgosha, R. Fortes-Patella and J. L. Reboud. Evaluation of the Turbulence Model Influence on the Numerical Simulations of Unsteady Cavitation. *J. of Fluids Engineering*. Vol. 125. 38-45, 2003.
- [7] B. Ji, X. W. Luo, R. E. A. Arndt and Y. L. Wu. Numerical simulation of three dimensional cavitation shedding dynamics with special emphasis on cavitation-vortex interaction, *Ocean Engineering*. Vol. 87. 64-77, 2014.
- [8] Y. Yamamoto, S. Watanabe and S. Tsuda. A Simple Cavitation Model for Unsteady Simulation and its Application to Cavitating Flow in Two-Dimensional Convergent-Divergent Nozzle. *IOP Conf. Ser.:Mater. Sci. Eng.* 72:022009, 2015.
- [9] G. Schnerr and J. Sauer. Physical and Numerical Modeling of Unsteady Cavitation Dynamics. *Proc. Fourth International Conference on Multiphase Flow*, 2001
- [10] Y. L. Young and B. R. Savander. Numerical Analysis of Large-Scale Surface-Piercing Propellers, *Ocean Engineering*. Vol. 38. 1368-1381, 2011.
- [11] E. Roohi, A. P. Zahiri and M. Passandideh-Fard. Numerical simulation of cavitation around a two-dimensional hydrofoil using VOF method and LES

turbulence model. *Applied Mathematical Modelling*. Vol. 37. 6469-6488, 2013

- [12] R. W. Schrage. Theoretical Study of Interphase Mass Transfer, *Columbia: ColumbiaUniversity Press*, 1953
- [13] S. Watanabe, K. Enomoto, Y. Hara and A. Furukawa. Observation of Unsteady Cavitating Flow in a Two-Dimensional Converging-Diverging Nozzle. *Proc. Fifth Int. Symp. on Fluid Machinery and Fluid Eng.* SS3-1, 2012.
- [14] S. Watanabe, W. Yamaoka and S. Tsuda. Unsteady Lift and Drag Characteristics of Cavitating Clark Y-11.7% Hydrofoil. *Proc. 27th IAHR Symp. on Hydraulic Machinery and Systems*, 2014
- [15] S. Watanabe, Y. Konishi, I. Nakamura and A. Furukawa. Experimental Analysis of Cavitating Behavior around a Clark Y Hydrofoil. *Proc. WIMRC 3rd International Cavitation Forum 2011*, 2011